The ER membrane protein complex is important for the biogenesis of flavivirus polyproteins

Ashley M Ngo[1], Matthew J Shurtleff[2], Katerina D Popova[2], Jessie Kulsuptrakul[1], Jonathan S Weissman[2,3], Andreas S Puschnik[1,4]

[1] Chan Zuckerberg Biohub, San Francisco, United States

[2] Department of Cellular and Molecular Pharmacology, University of California, San Francisco, San Francisco, United States

[3] Howard Hughes Medical Institute, University of California, San Francisco, San Francisco, United States

[4] Correspondence to: andreas.puschnik@czbiohub.org

Abstract

Flaviviruses such as dengue (DENV), Zika (ZIKV) or West Nile virus (WNV) translate their genome as a single multi-pass transmembrane (TM) protein at the endoplasmic reticulum (ER) membrane. Several genetic knockout (KO) screens identified the ER membrane protein complex (EMC) as a critical host component for flavivirus infection. The EMC facilitates accurate insertion, topology and/or stabilization of specific cellular TM proteins including a subset of tail-anchored proteins and G protein-coupled receptors. Here, we show that deletion of EMC in human cell lines decreased infection with DENV, ZIKV and WNV by 100 to 10,000-fold. Using replicon and immunoblotting studies in EMC KO cells, we demonstrated that the EMC was essential for viral protein expression. Ribosome Profiling of DENV-infected wild-type and EMC KO cells revealed no drastic differences in translation efficiency. Instead, absence of EMC led to a large fraction of expressed viral proteins being targeted to the proteasome post-translationally. We detected a decrease in stability in NS4A-NS4B of the viral polyprotein, a region rich in transmembrane domains. Additionally, we identified non-synonymous point mutations in NS4A and NS4B by

performing iterative passaging of DENV on EMC KO cells. Adaptive mutations rescued both viral replication and stable expression of the NS4A-NS4B polyprotein segment in EMC KO cells. Lastly, we showed a physical interaction between the EMC and DENV NS4B protein post-cleavage and rapid degradation of processed NS4B in the absence of EMC. Together, our results suggest that the EMC engages with DENV polyproteins to ensure proper biogenesis of the NS4A-NS4B region, and provide further evidence for the cellular function of the EMC in the stable expression of TM proteins.

Introduction

Flaviviruses such as dengue (DENV), Zika (ZIKV) or West Nile virus (WNV) express their genome as a single multi-pass transmembrane (TM) protein at the endoplasmic reticulum (ER) membrane. Subsequently, the polyprotein is cleaved by the viral NS2B-NS3 protease and the cellular signal peptidase into the individual structural (C, prM, E) and non-structural (NS1-5) proteins required for replication and assembly into new virions (Neufeldt et al., 2018). Similar to cellular TM proteins, the viral polyprotein relies on the host cell machinery for targeting to the ER, translocation across the membrane and insertion of transmembrane domains (TMDs) into the lipid bilayer during its translation. These processes are facilitated by the signal recognition particle (SRP), the translocon-associated protein (TRAP) complex (also known as signal-sequence receptor complex), the Sec61 translocon and the signal peptidase complex. These cell components were all identified as essential host factors for flavivirus infection in genetic screens underscoring their importance for virus replication (Krishnan et al., 2008; Marceau et al., 2016; Sessions et al., 2009; Zhang et al., 2016). For most TM proteins, recognition of a hydrophobic TMD or signal sequence by the SRP followed by transfer to the Sec61 translocation channel are sufficient for membrane targeting and accurate topogenesis (Shao and Hegde, 2011). Recently, it was shown that the ER membrane protein complex (EMC) plays a role in the insertion and/or stabilization of certain TM proteins (Chitwood et al., 2018; Guna et al., 2018; Shurtleff et al., 2018). Intriguingly, several

genome-wide CRISPR knockout (KO) screens for flavivirus dependency factors showed strong enrichment of the EMC (Ma et al., 2015; Marceau et al., 2016; Savidis et al., 2016; Zhang et al., 2016). However, its role in the virus life cycle is not yet understood.

The EMC was originally discovered in a genetic screen for yeast mutants modulating the unfolded protein response (UPR) (Jonikas et al., 2009). Genetic interaction mapping and biochemical purification revealed a six-subunit core complex (EMC1-6) conserved in yeast and mammals (Christianson et al., 2011; Jonikas et al., 2009). Other than its more general association with UPR and ER-associated degradation (ERAD), the EMC was shown to interact co-translationally and enable biogenesis of a subset of multi-pass TM proteins (Shurtleff et al., 2018). Biochemical characterization of select EMC-dependent TM proteins, such as tail-anchored proteins and G protein-coupled receptors (GPCRs), revealed that the EMC is capable of inserting TMDs into the ER membrane (Chitwood et al., 2018; Guna et al., 2018).

Here, we investigated how the mosquito-borne flaviviruses, DENV, ZIKV and WNV, depend on the EMC during infection. We showed that the EMC was required for DENV polyprotein biogenesis and identified a segment spanning NS4A-4B as the region dependent on the EMC for stable expression. Absence of the EMC resulted in post-translational degradation of viral proteins. Together, our data highlights how flaviviruses hijack important machinery for TM protein biogenesis to achieve optimal expression of their polyproteins, which reinforces a role for the EMC in stabilizing challenging TM proteins during synthesis.

Results

To validate the enrichment of EMC components in the flavivirus CRISPR screens, we generated isogenic EMC subunit KO cell lines in Huh7.5.1 and HEK293FT, two cell types that were used for the genetic screens (Figure S1A). Upon infection with DENV expressing Renilla luciferase (DENV-Luc), we measured a ~10,000-fold reduction in viral replication in Huh7.5.1 EMC1-6 KO cells (Figure 1A) and a 10-1,000-fold reduction in HEK293FT EMC1-5 KO cells (Figure 1B). The

differences in the extent of the phenotypes may be attributed to the presence of compensatory pathways or the degree of disruption of the entire protein complex between the two cell types upon knockout of a single subunit. The strong deficit in DENV replication in the absence of the EMC persisted over a 30-72h period (Figure S1B). Complementation of EMC2 and EMC4 KO cells with the respective cDNA completely restored levels of DENV infection (Figures 1C and S1C). Lastly, we tested the effect of EMC4 KO on several flaviviruses and saw a significant decrease of viral RNA for DENV, WNV and ZIKV but not hepatitis C virus (HCV), which is a more distantly related member of the *Flaviviridae* family (Figures 1D and S1D). This is congruent with results of an HCV CRISPR screen that did not identify the EMC as a critical host factor (Marceau et al., 2016). This finding highlights that there is a specific, evolutionarily conserved dependency on the EMC among mosquito-borne flaviviruses and not a universal disruption of trafficking to and/or translation or replication at the ER membrane, which would affect a wider range of viruses.

Next, we sought to determine at which step of the viral life cycle the EMC is required. As the EMC is important for the expression of a large set of TM proteins, its disruption leads to an altered cell surface proteome, which may affect viral entry. We measured effects on viral uptake in WT and EMC4 KO cells by quantifying the amount of internalized viral RNA at 2 and 6 hours post-infection (hpi), where we did not observe a difference (Figure 2A). Only at 24hpi, a timepoint when viral replication had occurred, was a difference in RNA load evident between WT and EMC4 KO cells. Furthermore, we used a DENV replicon expressing luciferase, which bypasses entry and does not produce viral particles, thus allowing the analysis of the effect of EMC KO specifically on translation and replication. In this assay, we saw decreased luminescence in EMC4 KO cells starting at 12 hours post-electroporation suggesting that the EMC is important during or prior to viral replication (Figure 2B). We additionally performed the replicon assay in the presence of MK-0608, a nucleoside analogue that inhibits the viral polymerase (Chen et al., 2015), and observed that the luminescence signal in EMC4 KO cells was lower than in replication-inhibited WT cells

suggesting that deletion of EMC has an effect on viral translation, which happens prior to replication (Figure S2A). To further dissect effects on translation or genome replication of DENV, we conducted an immunoblot timecourse series, where WT and EMC4 KO cells were infected at a high multiplicity of infection (moi=32) and lysates were harvested at early timepoints post-infection (6-12hpi), when no or only little DENV replication had occurred. Viral protein expression was lower in EMC4 KO compared to WT cells as early as 6hpi further supporting a translation defect (Figures 2C and S2B). To rule out any contribution of low levels of replication to the observed phenotype, we also performed the immunoblot experiment in the presence of MK-0608 and still saw different amounts of DENV protein accumulation between WT and EMC4 KO cells indicating that the EMC is indeed important for viral protein expression (Figures S2C and S2D). Interestingly, while the EMC has been implicated in the stable biogenesis of TM proteins, we found reduced expression of both TMD and non-TMD containing viral proteins. This suggests that the defect likely occurs at the polyprotein stage thus affecting all individual, cleaved proteins.

The expression of flaviviral proteins is a complex process that requires several steps. DENV translation is initiated in a cap-dependent manner, whereupon the single-stranded positive-sense RNA genome is translated into a single ~3,400 amino acid long multi-pass TM protein. This polyprotein is co- and post-translationally processed by host and viral proteases producing the individual functionally active structural and non-structural proteins. We first tested whether the defect occurs at the stage of polyprotein translation. We used ribosome profiling (Ribo-seq), which measures the density of ribosomes on a given mRNA species with high positional resolution, to compare translation efficiencies (TE) and successful full-length synthesis of both cellular and viral proteins in WT and EMC4 KO cells (Ingolia et al., 2009). Any changes in TE or premature ribosome stalling in EMC KO vs WT cells would be reflected by changes in ribosomal footprints (as measured by Ribosome profiling) normalized to changes in mRNA abundance (as measured by RNA-seq). In the uninfected condition, we did not observe dramatic changes in TE

for cellular mRNAs in EMC4 KO vs WT cells (Figure 3A and Supplementary Table 1). This is in line with previously reported results using CRISPRi knockdown against EMC subunits suggesting that deletion of EMC minimally impacts the synthesis rates of its client proteins (Shurtleff et al., 2018). Similarly, we did not find any substantial differences in viral TE in EMC4 KO cells relative to WT cells at 18 (0.43x) and 44hpi (2.17x) (Figures 3B and 3C and Supplementary Table 1). Instead, we observed that DENV RNA was among the highest translated (top 0.1%) mRNAs in both WT and EMC4 KO cells (Figure S3A). The lower number of ribosomal footprints aligning to the viral genome in EMC4 KO cells was largely due to the reduced number of viral RNA copies present in the cells. Moreover, footprints were found to map throughout the viral genome in EMC4 KO cells, indicating that synthesis of full-length polyprotein still occurred (Figure S3B). Therefore, we concluded that translation of DENV polyproteins is not strongly impacted by loss of EMC, which led us to explore potential post-translational defects.

Proper insertion of TMDs and correct folding are required for stable expression of TM proteins, while misfolded proteins are generally targeted to the proteasome for degradation via the ERAD pathway (Olzmann et al., 2013). To probe whether an increased fraction of viral proteins is degraded by the proteasome in EMC deficient cells, we infected WT and EMC4 KO cells with DENV in the presence of Bortezomib (BZ), a proteasome inhibitor, thus preventing removal of misfolded proteins from the cells. Indeed, BZ treatment led to an increase of detectable viral proteins in EMC4 KO cells but not WT cells (Figure 3D). Addition of BZ, however, did not restore DENV replication arguing that the proteasome-targeted proteins are non-functional (Figure S3C). Together, this suggests that in the absence of EMC viral proteins are still translated but are unable to achieve a stable conformation resulting in their degradation and inability to establish efficient replication.

For cellular multi-pass client proteins, such as transporters and GPCRs, the EMC co-translationally engages with specific TMDs in order to support insertion into the membrane and

allow stable expression of the entire TM protein (Chitwood et al., 2018; Shurtleff et al., 2018). We used two orthogonal methods, a fluorescence-based protein stability assay and viral evolution, to examine which region of the viral polyprotein requires the EMC for successful expression. First, we utilized a dual-color fluorescent reporter as previously described (Chitwood et al., 2018). The C terminus of different segments of the DENV polyprotein was fused to eGFP followed by a viral T2A sequence and mCherry (G2C) (Figure 4A). Translation of the fusion constructs generates two protein products at a 1:1 ratio due to peptide bond skipping by the ribosome at the T2A site: 1) a polyprotein segment fused to eGFP and 2) mCherry. Any post-translational instability of the eGFP fusion protein due to misfolding results in an eGFP:mCherry ratio of less than 1. As expected, the cytosolic G2C-only construct displayed a 1:1 ratio in both WT and EMC4 KO cells, while the β_1-adrenergic receptor (ADRB1) fused to G2C exhibited drastic destabilization in EMC4 KO compared to WT cells as was previously reported (Figure 4B) (Chitwood et al., 2018). Applying this approach to different DENV polyprotein G2C fusion constructs, we observed that the segments containing only the structural proteins (capsid, prM and E) or NS1-3 were not destabilized in EMC4 KO Huh7.5.1 cells (Figure 4B). By contrast, constructs encoding both NS4A and NS4B (but not either of them alone) showed reduced stability in EMC4 KO cells (Figure 4B). Similar results were obtained in HEK293FT (Figure S4). NS4A has 3 TMDs with the third (termed 2K peptide) being highly hydrophobic and serving as a signal sequence for the translocation of NS4B into the ER membrane (Lin et al., 1993). Subsequently, the NS4A-2K junction is cleaved by the viral protease and the 2K-NS4B junction by the signal peptidase. As the 2K-targeted NS4B-5-G2C construct did not display a stability defect in EMC deficient cells, the results suggest that EMC mediates stable expression by first engaging within NS4A prior to the 2K peptide and that a defect in NS4A topogenesis is extended to the NS4B region. Stability of NS4A-4B-G2C was restored to near WT levels by complementation of EMC4 KO cells with EMC4 cDNA (Figure 4C). Moreover, treatment of EMC4 KO cells with BZ increased the eGFP:mCherry ratio of NS4A-4B-G2C in EMC4 KO cells indicating that this region of the polyprotein is misfolded and targeted for

183 degradation in the absence of EMC (Figure 4D). Therefore, we linked the DENV replication
184 phenotype in EMC deficient cells to a specific molecular defect in the NS4A-4B region of the
185 polyprotein.
186
187 In a second, orthogonal approach, we performed viral adaptation to evolve EMC-independent
188 DENV mutants by passaging the virus consecutively on EMC4 KO Huh7.5.1 cells every 3-4 days.
189 After 20-22 passages we observed cell death in 3 out of 6 independent adaptation experiments.
190 Sequencing of RNA extracted from supernatant and alignment to the WT16681 DENV genome
191 revealed two non-synonymous point mutations in NS4A and NS4B, which were conserved across
192 all three isolates (Figure 5A). The A6665G mutation led to a tyrosine to cysteine and the A7558T
193 mutation to an asparagine to tyrosine substitution. The majority of other SNPs was silent (Figure
194 S5). A6665G is predicted to be inside a TMD helix encoding region of NS4A suggesting that this
195 TMD relies on the EMC for proper ER membrane insertion (Miller et al., 2007). Only one of 1,359
196 DENV serotype 2 genomes from the NCBI database has a G at this position encoding cysteine,
197 while other sequences all encode tyrosine. This evolutionary conservation suggests that this
198 residue indeed has an important function. Similarly, the frequency of A at position 7558 is very
199 conserved with 99.6%, and there is no T encoding tyrosine in the 1,359 sequenced strains.
200 Interestingly, A7558T resides in a non-TMD region at the end of NS4B, thus likely supporting
201 membrane insertion or folding in a different manner (Miller et al., 2006). To demonstrate that the
202 acquired mutations confer independence from EMC, we infected WT and EMC4 KO cells with
203 WT16681 or the three evolved DENV isolates and measured replication. WT16681 DENV
204 displayed a ~100-fold decrease in viral RNA in EMC4 KO relative to WT cells, while the EMC
205 adapted isolates had equal RNA levels (Figure 5B). To dissect whether both mutations are
206 required for optimal replication in EMC KO background, we introduced them individually or in
207 tandem into the DENV-Luc infectious clone and generated virus. While A6665G and A7558T
208 individually restored DENV replication in EMC4 KO cells to 30 and 86% of WT levels, respectively,

209 the double mutant displayed complete rescue of viral growth (Figure 5C). We also introduced the
210 two adapted mutations into NS4A-5-G2C, which showed increased stability in EMC4 KO cells
211 compared to the WT construct thus reverting the molecular destabilization phenotype (Figure 5D).
212 Remarkably, the G2C fluorescence assay and viral adaptation independently pinpointed NS4A-
213 4B of the polyprotein as the region which requires the EMC. The results of the two experiments
214 suggest that a defect in the stable insertion of the NS4A TMD2 could lead to subsequent failure
215 in accurate topogenesis and/or stability of NS4B. By contrast, polyprotein segments starting with
216 2K-NS4B were stably expressed in EMC KO cells as was shown using NS4B-5-G2C construct
217 (Figure 4A). Therefore, the EMC is required for correct insertion, processing and/or folding of the
218 NS4A-4B region.
219
220 Finally, to probe how absence of EMC causes failure of DENV replication, we transfected a
221 subgenomic NS2B-4B construct (containing functional NS2B-NS3 for polyprotein cleavage) with
222 C terminal fusion to eGFP into WT and EMC4 KO cells and immunoblotted against the different
223 processed products. While there was no notable difference between the higher molecular weight
224 intermediates (NS2B-NS3-NS4A-NS4B-eGFP or NS4A-NS4B-eGFP), we observed reduced
225 accumulation of processed NS4B-eGFP in EMC4 KO cells (Figure 6A). BZ treatment indicated
226 rapid degradation of cleaved NS4B-eGFP in EMC deficient cells. Furthermore, if the EMC acts to
227 insert or stabilize NS4A-4B, we hypothesized that direct binding of NS4B to EMC post polyprotein-
228 processing should be detectable in WT cells. We performed a co-immunoprecipitation using
229 FLAG-tagged EMC4 and detected NS4B but not prM or NS5 in the pulldown (Figure 6B). Overall,
230 this supports the finding that EMC physically engages with NS4A-4B to facilitate its biogenesis
231 and stable expression.
232
233

Discussion

Based on our results and previous work (reviewed in Chitwood and Hegde, 2019) we propose the following model for the role of the EMC in flavivirus infection. During translation of the polyprotein the EMC engages with TMDs in NS4A and NS4B to facilitate their biogenesis, correct folding and stable expression (Figure 6C). In the absence of the EMC, TMDs in the NS4A-4B region are not stably or accurately integrated in the ER membrane leading to misfolding and degradation of processed NS4B (and potentially also NS4A). NS4A and NS4B fulfill crucial functions for viral replication. NS4A induces ER membrane rearrangements important for the formation of viral replication complexes (Miller et al., 2007; Roosendaal et al., 2006) while NS4B interacts with the NS3 helicase and also suppresses the cellular interferon response (Muñoz-Jordán et al., 2005; Zou et al., 2015). It remains to be studied whether the other viral proteins are destabilized due to an overall topology defect in the NS4A-4B region of the polyprotein or if lack of functional NS4A and/or NS4B inside the replication complexes results in instability of all viral proteins.

In addition to characterizing the role of the EMC in the viral life cycle, our data also helps to further elucidate its cellular function. The emerging role of the EMC to facilitate topogenesis has been implicated for several cellular TM proteins (Chitwood et al., 2018; Coelho et al., 2019; Guna et al., 2018; Shurtleff et al., 2018; Volkmar et al., 2019). For a subset of tail-anchored proteins, the EMC inserts the sole C-terminal TMD after translation is completed in the cytosol (Guna et al., 2018). Moreover, the EMC co-translationally inserts the first N-terminal TMD of many GPCRs with an N_{exo} topology (N terminus in the ER lumen) (Chitwood et al., 2018). By contrast, we found EMC-dependency within DENV NS4A-4B, a region with several TMDs, which are not close to the termini of the polyprotein. This provides experimental evidence that the EMC is not only capable of supporting stable expression of TMDs near the N and C termini but also of internal TMDs, arguing that the EMC may directly facilitate the biogenesis of a wide variety of implicated TM proteins beyond tail-anchored proteins and GPCRs (Shurtleff et al., 2018). Additionally, it is noteworthy that the DENV polyprotein is distinct from human TM proteins in that it contains

multiple signal peptidase cleavage sites along the polyprotein, including at the 2K/NS4B site between NS4A and NS4B, which removes the 2K peptide acting as signal sequence for NS4B (Lin et al., 1993; Miller et al., 2006). Interestingly, it was shown (e.g. for ADRB1) that addition of a signal sequence or an N_{cyt} TMD upstream of the first N_{exo} TMD makes the EMC dispensable for biogenesis (Chitwood et al., 2018). This observation suggests that EMC-mediated integration/stabilization of TMDs may be context-dependent. It needs to be elucidated whether the EMC plays an active role in the TMD insertion of the DENV polyprotein into the ER membrane or whether it functions as a post-insertional chaperone for specific TMDs.

Generally, for both cellular multi-pass TM proteins and the DENV polyprotein, only one or a subset of TMDs seem to require the EMC for accurate topogenesis, while the other TMDs rely on the Sec61 translocon. The exact interplay between Sec61 and the EMC during TM protein biogenesis warrants further investigation. The simultaneous dependency of flaviviruses on both Sec61 and EMC as highlighted by the CRISPR KO screens could allow an in-depth analysis of the sequence and TMD features that may determine membrane insertion via Sec61 or EMC.

The A6665G mutation is predicted to be in a TM helix of NS4A but A7558T is not in a TM region (Miller et al., 2006, 2007). Therefore, further studies are necessary to determine the exact interaction between the EMC and the viral TMDs. Interestingly, the A6665G mutation also arose during DENV adaptation to cell lines deficient in the oligosaccharyltransferase (OST) complex, another critical host factor inside the ER membrane (Marceau et al., 2016; Puschnik et al., 2017). The OST complex has been shown to be important for RNA genome replication in a catalytically independent function and was suggested to act as structural scaffold for viral replication complexes. It is possible that the tyrosine to cysteine substitution generally modulates ER anchoring of NS4A. Overall, it remains to be elucidated how the resulting amino acid substitutions rescue stable expression of NS4A and NS4B.

The isolation of EMC-independent DENV mutants additionally enables drug screening for EMC modulators by testing compounds against WT DENV-Luc and then counter-screening hits with

EMC-adapted virus. EMC inhibitors may be a useful chemical tool to study EMC function and also provide a potential antiviral therapeutic against flaviviruses. Host-directed antivirals may have the advantage of a broader activity against multiple viruses and a higher barrier of drug resistance. Only 50% of the adaptation experiments yielded escape mutants containing two mutations after >20 passages. For comparison, for direct-acting antivirals (e.g. viral polymerase inhibitors), one point mutation is often sufficient to overcome the mechanism of action (Beaucourt and Vignuzzi, 2014).

Lastly, the EMC was originally discovered to be associated with the UPR (Jonikas et al., 2009), and upregulation of UPR during flavivirus infection has been reported (Peña and Harris, 2011; Reid et al., 2018; Su et al., 2002). It is possible that competition between viral polyproteins and cellular proteins for the machinery important for proper TM protein expression (such as EMC, OST complex and ERAD components) is linked to this phenomenon. The induction of ER stress can further trigger autophagy, which has also been shown to be beneficial for flavivirus infection (Abernathy et al., 2019; Lee et al., 2018; Senft and Ronai, 2015). Therefore, hijacking the EMC may have direct and indirect implications for flavivirus replication.

Overall, our study gives detailed insights into how flaviviruses exploit the EMC to support proper polyprotein expression, and we provide further evidence for the cellular function of the EMC in TM protein topogenesis by utilizing DENV as a cell biological tool.

Acknowledgments

We like to thank the following people: Jan Carette for discussions, providing reagents and critically reading the manuscript; Caleb Marceau for technical advice and providing reagents; members of the Biohub Infectious Disease Initiative and the Weissman lab for discussions and technical advice; the Biohub Genomics Platform for help with sequencing. ASP was supported by the Chan Zuckerberg Biohub. MJS is a Howard Hughes Medical Institute Fellow of the Helen Hay Whitney Foundation and JSW is an Investigator of the Howard Hughes Medical Institute.

312

313 **Author contributions**

314 ASP and JSW conceptualized study. AMN and ASP conducted the majority of experiments with

315 help from JK. MJS and KDP performed ribosome profiling. ASP wrote the manuscript with input

316 from all authors.

317

318

319

Figure 1

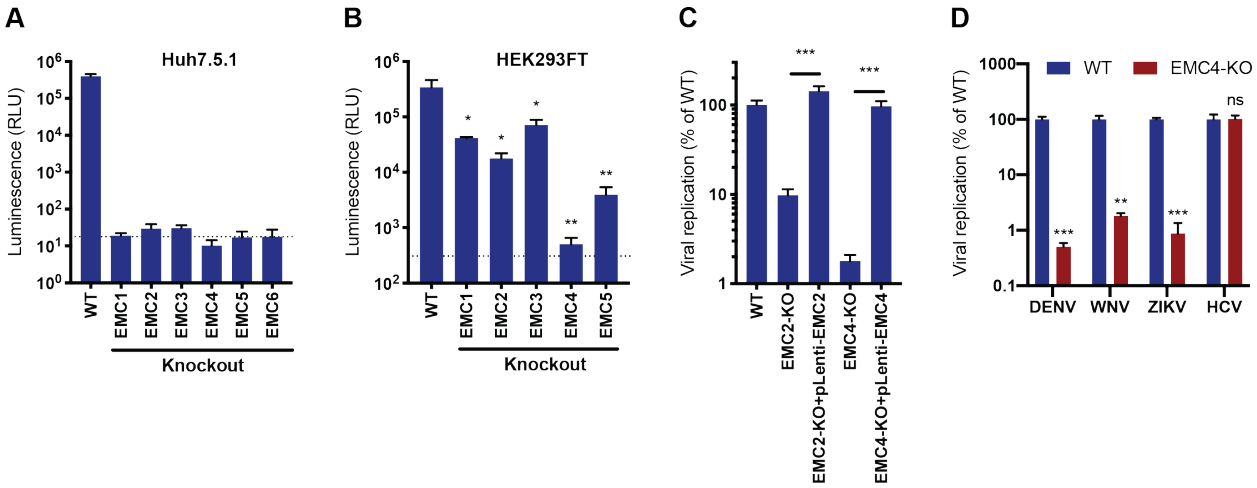

Figure 1: EMC is required for flavivirus infection

(A) Luminescence of WT and EMC subunit KO Huh7.5.1 cells infected with DENV-Luc at 30hpi. Dotted line is background from uninfected control.

(B) Luminescence of WT and EMC subunit KO HEK293FT cells infected with DENV-Luc at 48hpi. Dotted line is background from uninfected control.

(C) Replication of DENV-Luc in WT, EMC2- and EMC4-KO, and cDNA complemented KO HEK293FT cells.

(D) Quantitative RT-PCR of DENV, WNV, ZIKV and HCV RNA in WT or EMC4-KO Huh7.5.1 cells.

In all figures, values are shown as mean of three biological replicates with standard deviation in (A)-(C) and mean with standard error of the mean in (D). *t*-tests were performed to determine statistical significance and *p*-values are defined as ns=non-significant, *<0.05, **<0.01, ***<0.001.

Figure 2

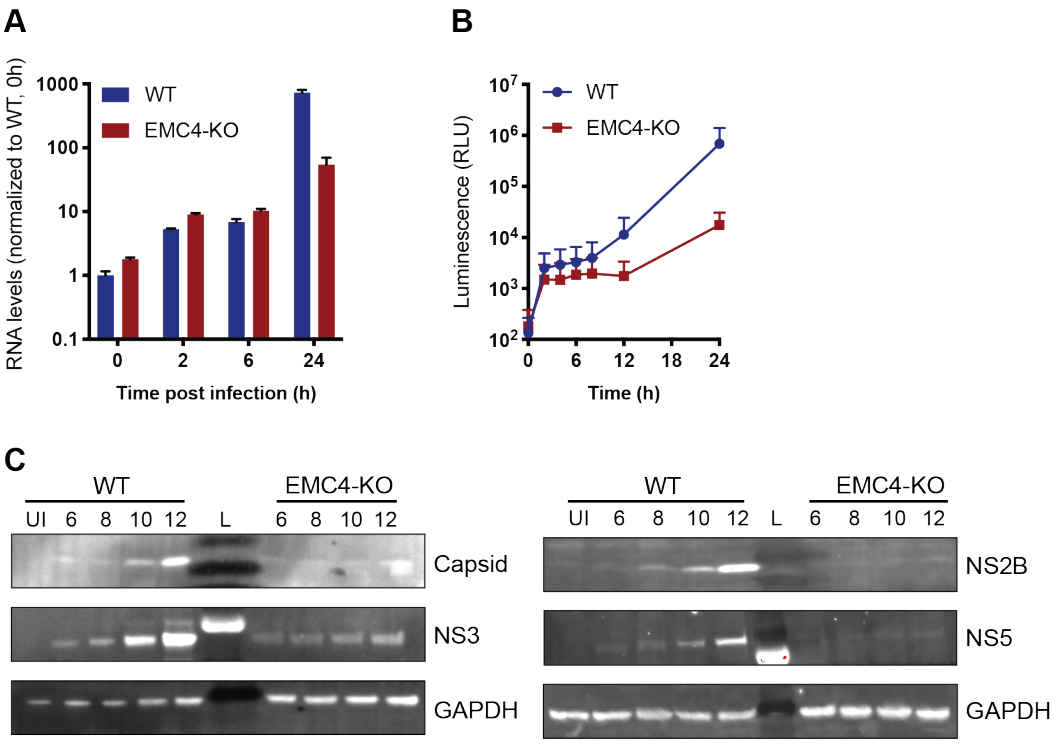

Figure 2: EMC is important for optimal viral protein expression

(A) Quantitative RT-PCR of internalized DENV RNA in WT and EMC4-KO Huh7.5.1 cells at different timepoints post-infection. The data is from three biological replicates and shown as mean with standard error of the mean.

(B) Luminescence of WT and EMC4-KO HEK293FT cells, which were electroporated with DENV replicon expressing Renilla luciferase and collected at different times post-electroporation. The data is from three biological replicates for each timepoint and shown as mean with standard deviation.

(C) Immunoblot analysis of DENV infected WT and EMC4-KO HEK293FT cells at different timepoints post-infection (6/8/10/12h). Lysates were blotted for different viral proteins (Capsid, NS2B, NS3 and NS5) and GAPDH was used as loading control. UI=uninfected control; L=ladder. Quantification of bands is shown in Figure S2B.

Figure 3

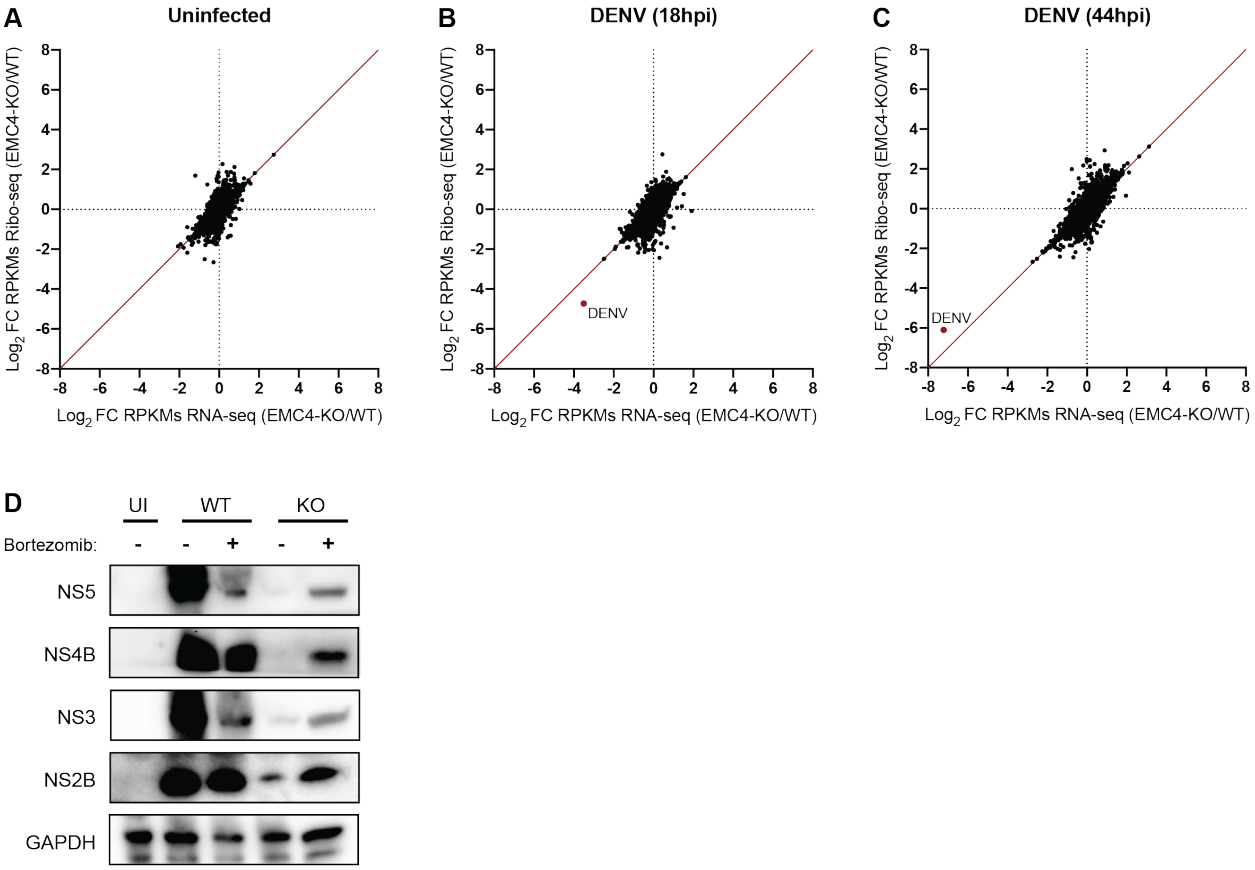

Figure 3: EMC knockout does not largely affect viral translation efficiency but leads to post-translational protein degradation

(A) Ribosome Profiling (Ribo-seq) and RNA-seq were performed in uninfected WT and EMC4-KO HEK293FT cells to measure changes in translation efficiency (TE). Log_2 fold-change (FC) of reads per kb of transcript, per million mapped reads (RPKMs) between EMC4-KO and WT cells for Ribosome Profiling and RNA-seq are displayed on the y- and x-axis, respectively. Each dot represents one RNA transcript. Fold-change in TE for a given transcript is defined as the change in Ribosome Profiling RPKMs normalized to the change in RNA-seq RPKMs. The red line represents fold-change of TE=1.

(B) Ribosome Profiling (Ribo-seq) and RNA-seq were performed in DENV-infected WT and EMC4-KO HEK293FT cells 18h post-infection to measure changes in translation efficiency (TE). The DENV transcript is highlighted in red. The red line represents fold-change of TE=1.

(C) Ribosome Profiling (Ribo-seq) and RNA-seq were performed in DENV-infected WT and EMC4-KO HEK293FT cells 44h post-infection to measure changes in translation efficiency (TE). The DENV transcript is highlighted in red. The red line represents fold-change of TE=1.

(D) Immunoblot analysis of DENV infected WT and EMC4-KO HEK293FT cells with or without addition of bortezomib (50nM), a proteasome inhibitor at 18hpi. GAPDH was used as loading control. UI=uninfected.

Figure 4

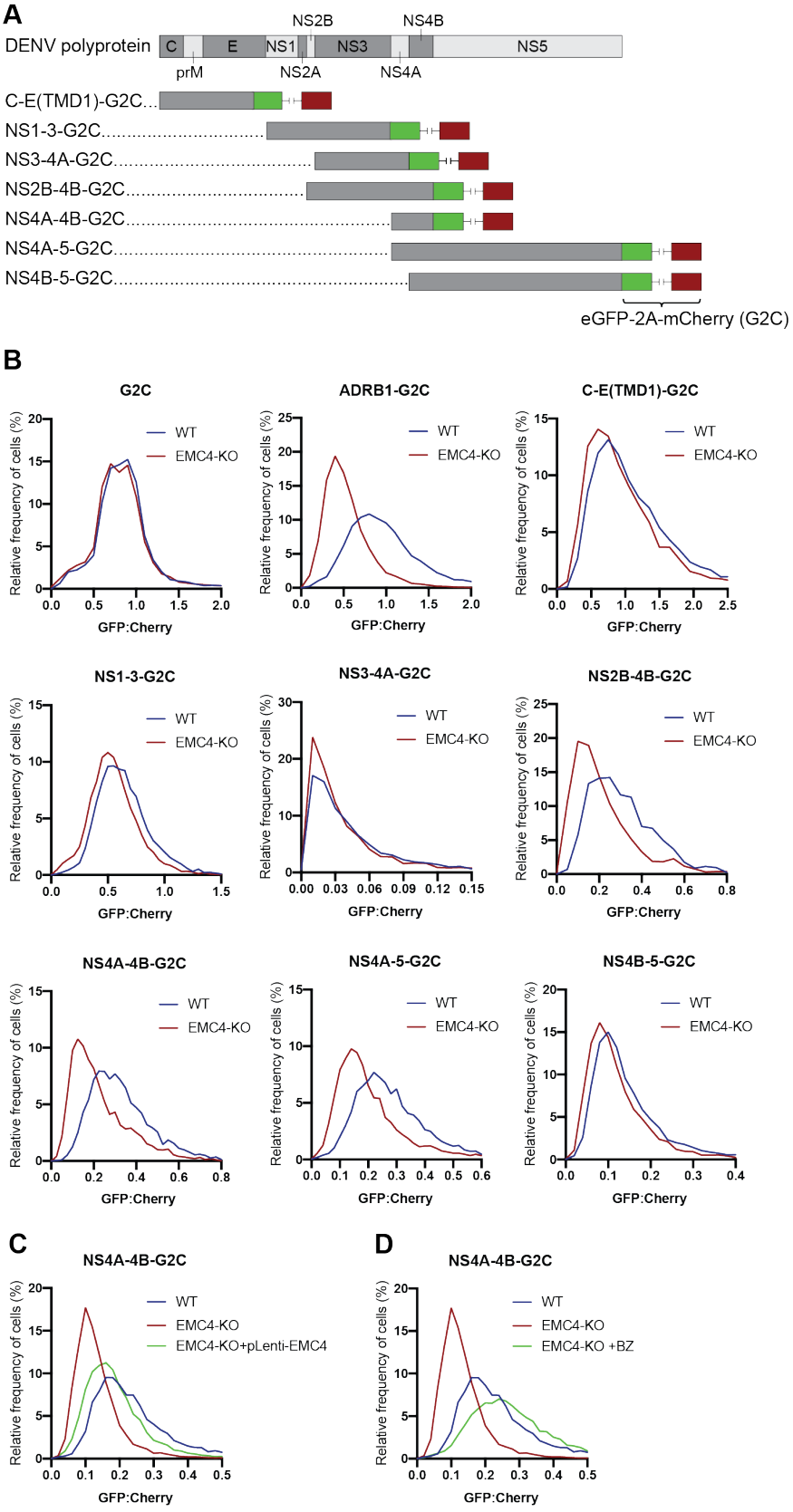

Figure 4: EMC is required for proper biogenesis of the NS4A-NS4B region of the DENV polyprotein

(A) Overview of dual-fluorescence reporter constructs of DENV polyprotein for analysis of protein stability. Segments of the DENV genome encoding parts of the polyprotein were cloned with a C-terminal fusion to eGFP-T2A-mCherry (G2C). The T2A peptide leads to peptide bond skipping during translation resulting in two protein products, DENV protein fused to eGFP and mCherry. The GFP:mCherry fluorescence ratio reflects changes in DENV protein stability.

(B) Flow cytometry measurements of GFP:mCherry fluorescence ratio for G2C constructs in WT and EMC4-KO Huh7.5.1 cells. The fluorescence ratios are depicted as histograms. ADRB1=β1-adrenergic receptor.

(C) Measurement of GFP:mCherry fluorescence ratio of NS4A-4B-G2C construct in WT, EMC4-KO and EMC4 cDNA complemented EMC4-KO HEK293FT cells.

(D) Measurement of GFP:mCherry fluorescence ratio of NS4A-4B-G2C construct in WT, EMC4-KO and bortezomib-treated EMC4-KO HEK293FT cells. Note that (C) and (D) use same WT and EMC4-KO data as experiments were performed in parallel.

Figure 5

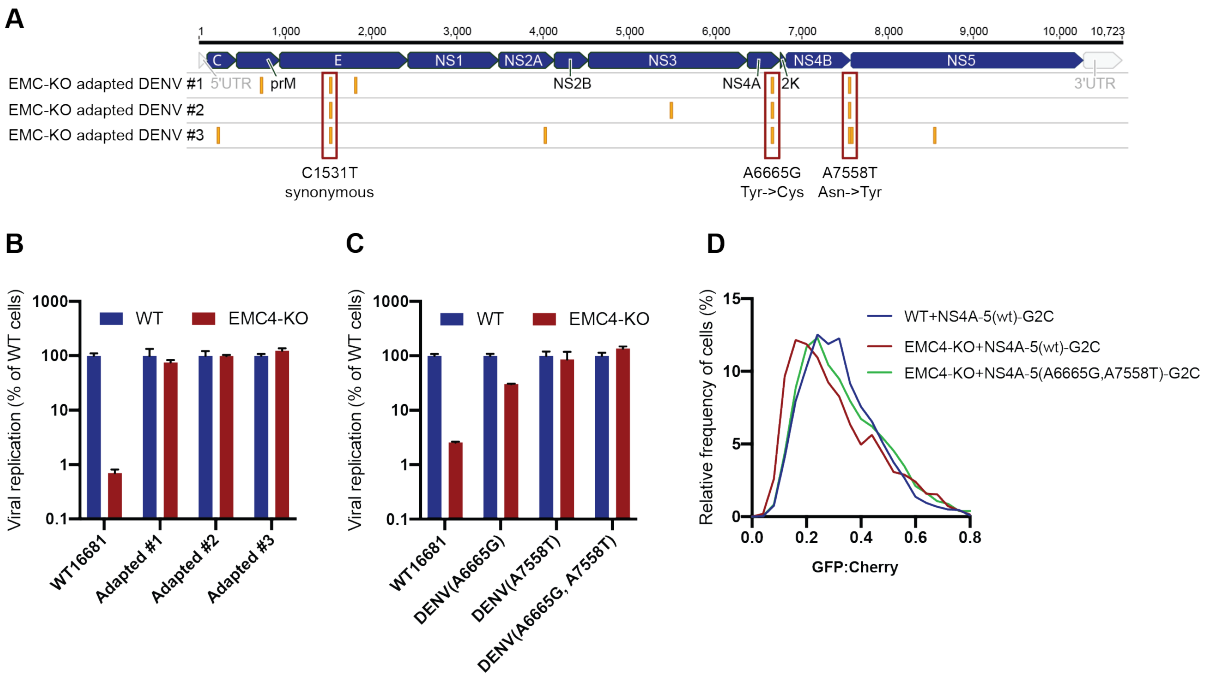

Figure 5: Adaptation of DENV to EMC KO cells reveals non-synonymous point mutations in NS4A and NS4B

(A) Identification of SNPs in EMC4-KO adapted DENV relative to DENV 16681 reference genome by next-generation sequencing of supernatant-extracted viral RNA. Mutations common across all three replicates are highlighted by red boxes and their nucleotide and amino acid changes are shown below. A table of all identified SNPs can be found in Figure S5.

(B) Quantitative RT-PCR of DENV RNA from WT DENV 16681 and the three isolated EMC-adapted DENV in WT and EMC4-KO Huh7.5.1. The data is from three biological replicates and shown as mean with standard error of the mean.

(C) Viral infection assay in WT and EMC4 KO Huh7.5.1 using WT DENV-Luc or mutant DENV-Luc containing A6665G and A7558T either individually or in tandem. The data is from three biological replicates and shown as mean with standard deviation.

(D) Measurement of GFP:mCherry fluorescence ratio of WT NS4A-5-G2C and NS4A-5(A6665G,A7558T)-G2C constructs in WT and EMC4-KO Huh7.5.1.

Figure 6

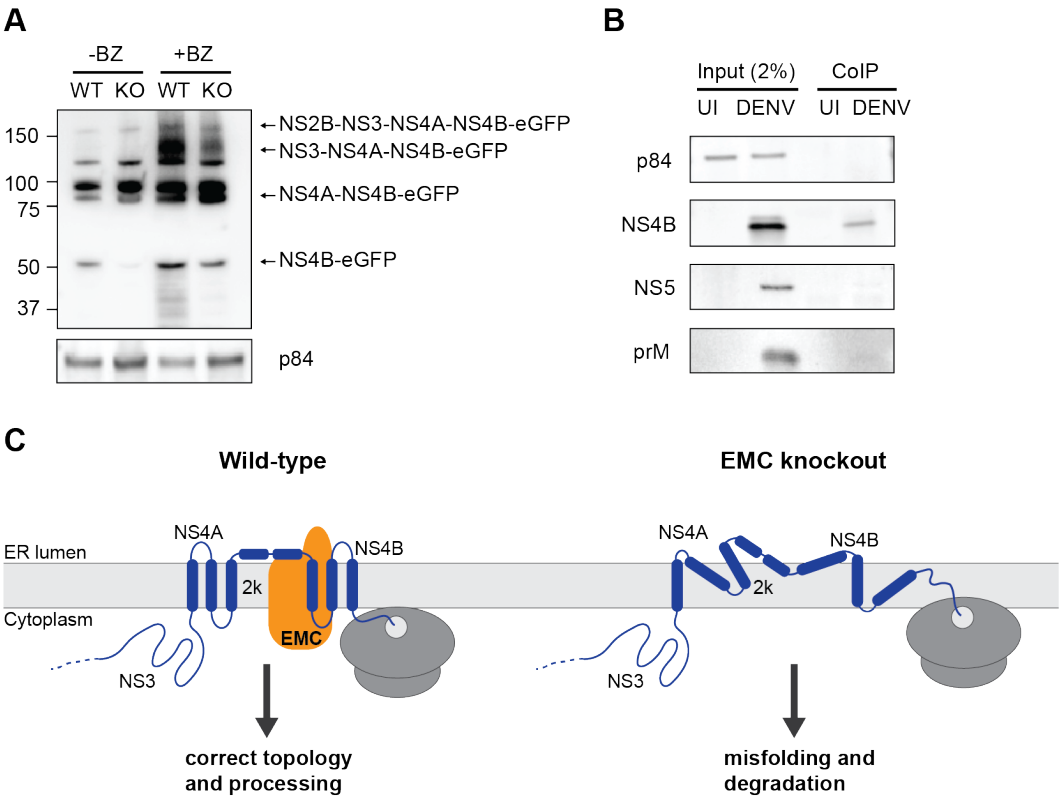

Figure 6.: EMC physically interacts with DENV NS4B post-cleavage and absence of EMC leads to rapid degradation of misfolded NS4B.

(A) Immunoblot for processed products of transfected NS2B-4B-GFP construct in WT and EMC4 KO cells in presence or absence of BZ. p84 was used as loading control.

(B) Co-immunoprecipitation of EMC4-FLAG from lysates of uninfected (UI) or DENV infected HEK293FT EMC4-FLAG cells followed by immunoblotting against viral proteins (prM, NS4B, NS5). p84 was used as loading and non-specific binding control.

(C) Model for the role of EMC in DENV infection. In DENV infected wild-type cells, the EMC co-translationally engages with NS4A and/or NS4B TMDs to facilitate correct/stable insertion ensuring a functional topology. In the absence of the EMC, misfolding of the NS4A-NS4B region occurs during polyprotein synthesis resulting in degradation of viral proteins.

Figure S1

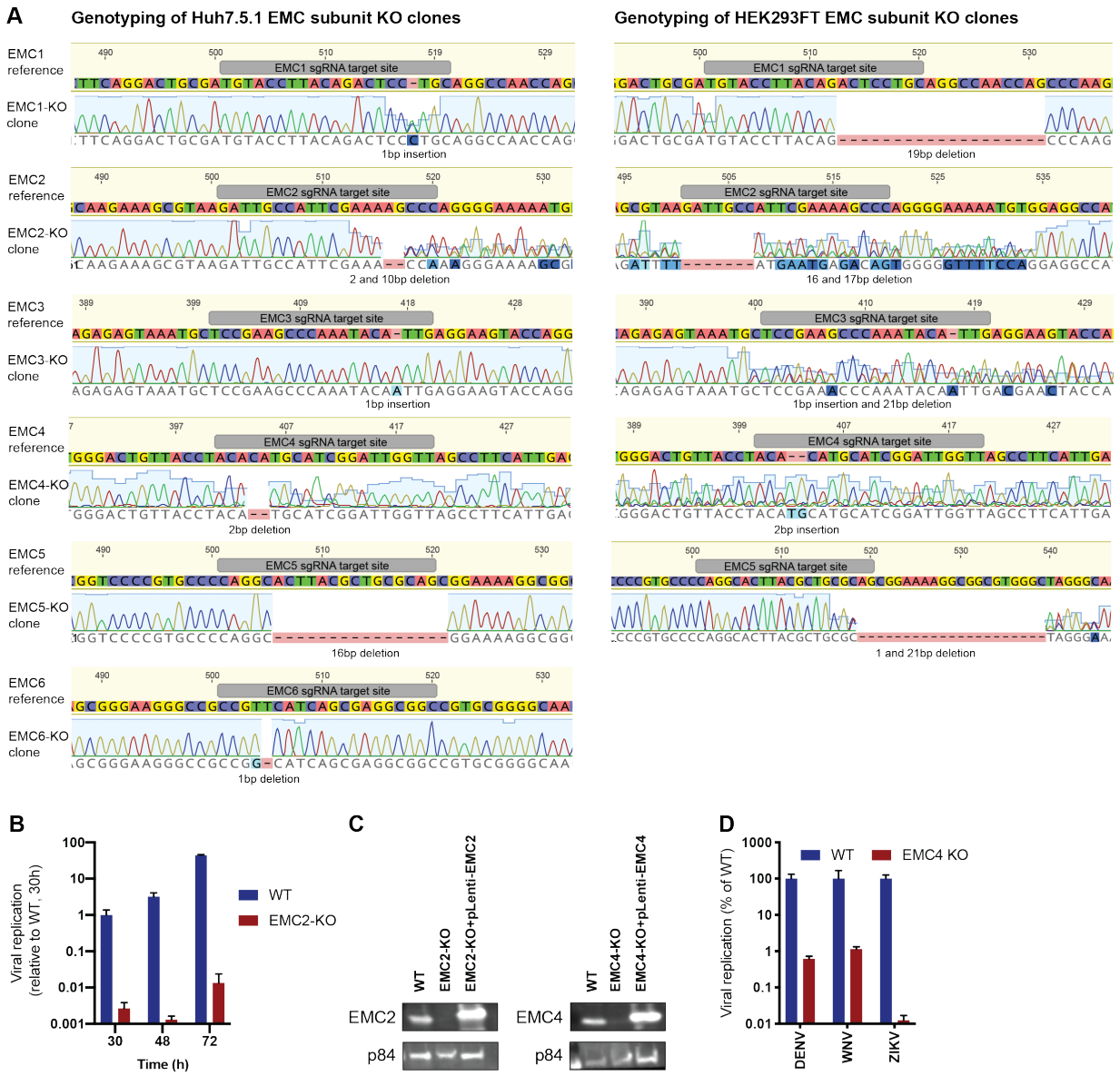

Figure S1: EMC is required for flavivirus infection

(A) Sanger sequencing of clonal EMC subunit KO Huh7.5.1 and HEK293FT cells. sgRNA targeting site is highlighted in reference sequence (top) and indel mutation is shown below sequencing trace of KO cells. For heterozygous mutants, TIDE was used to determine indel mutations.

(B) Quantitative RT-PCR of DENV RNA in WT or EMC2-KO Huh7.5.1 at 30, 48 and 72h post infection. Values are shown relative to the WT, 30h condition.

(C) Immunoblot analysis of EMC2 or EMC4 expression in WT, EMC2- and EMC4-KO, and cDNA complemented KO HEK293FT cells. p84 was used as loading control.

(D) Quantitative RT-PCR of DENV, WNV and ZIKV RNA in WT or EMC4-KO HEK293FT cells. For QPCR experiments, values are shown as mean of three biological replicates with standard error of the mean.

Figure S2

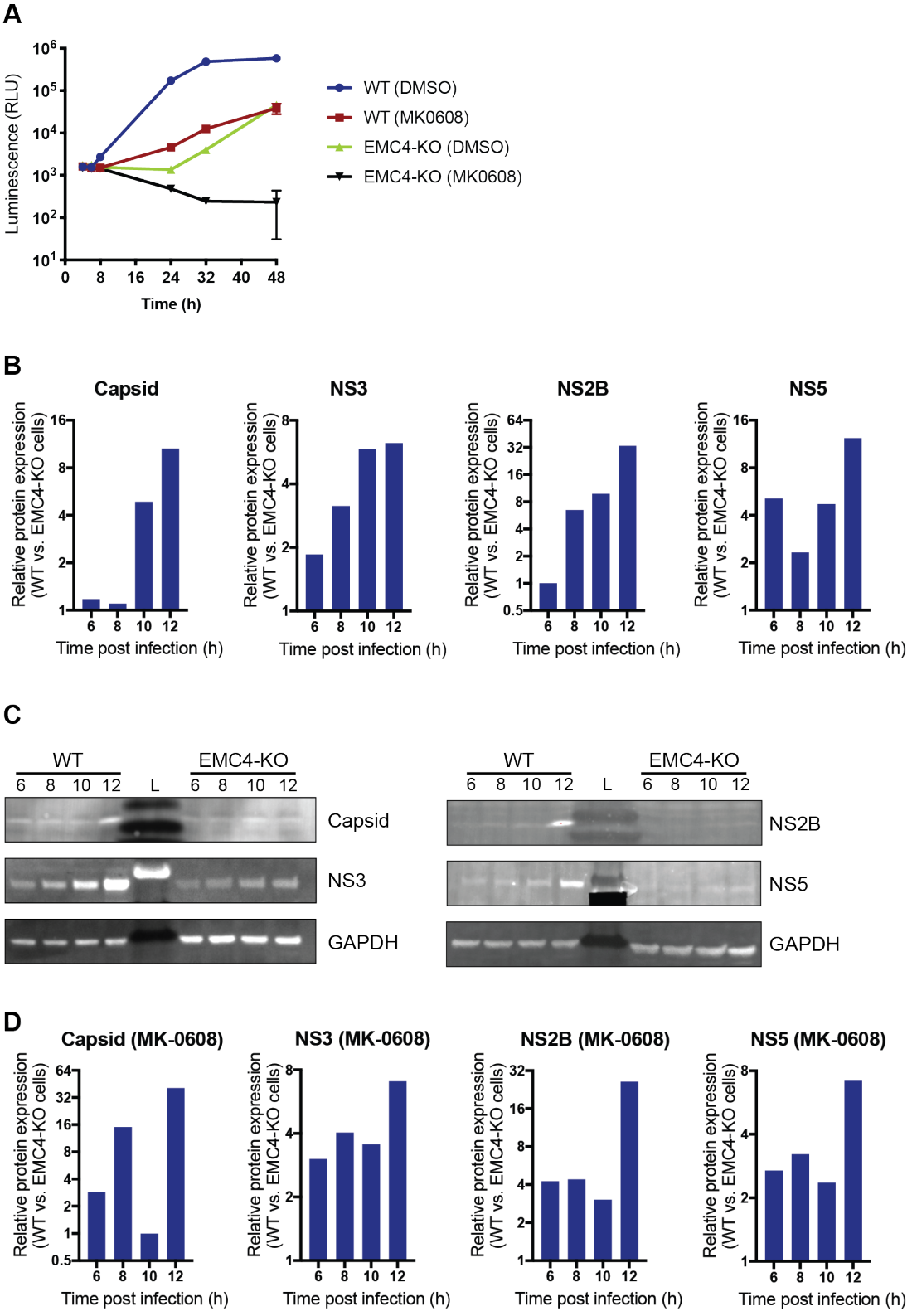

Figure S2: EMC is important for optimal viral protein expression

(A) Luminescence of WT and EMC4-KO cells electroporated with DENV replicon expressing Renilla luciferase and treated with MK-0608 (a nucleoside analogue, which inhibits the DENV polymerase) or DMSO. Lysates were collected at different times post electroporation. The data is from three biological replicates and shown as mean with standard deviation.

(B) Quantification of viral protein expression in EMC4-KO cells relative to WT cells by densitometry. Bands of viral proteins from Figure 2C were quantified and normalized to GAPDH bands at each timepoint.

(C) Immunoblot analysis of DENV infected WT and EMC4-KO HEK293FT cells at different timepoints post-infection (6/8/10/12h) with treatment of MK-0608 to inhibit viral replication. Lysates were blotted for different viral proteins (Capsid, NS2B, NS3 and NS5) and GAPDH was used as loading control. UI=uninfected control; L=ladder. Quantification of bands is shown in Figure S2D.

(D) Quantification of viral protein expression in EMC4-KO cells relative to WT cells by densitometry. Bands of viral proteins from Figure S2C were quantified and normalized to GAPDH bands at each timepoint.

Figure S3

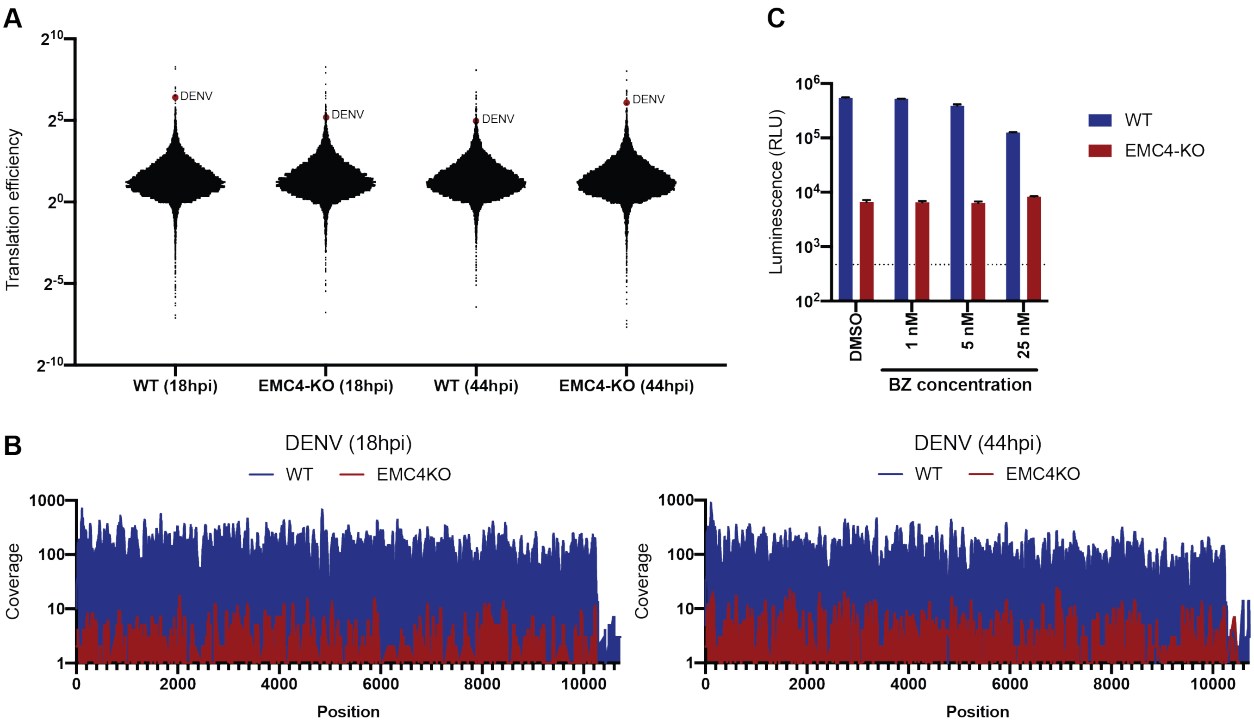

Figure S3: EMC knockout does not largely affect viral translation efficiency but leads to post-translational protein degradation

(A) Translation efficiencies (ribosome densities per RNA molecule) of cellular and DENV mRNA in WT and EMC4-KO cells at 18 and 44hpi. DENV is highlighted as red dot.

(B) Footprint distribution of Ribosome Profiling reads mapped to the DENV genome in WT and EMC4-KO cells at 18 and 44hpi. Nucleotide position of DENV genome is indicated on x-axis.

(C) DENV-Luc infection of WT and EMC4 KO HEK293FT cells treated with DMSO control or different concentrations of BZ for 24h. Dotted line indicates background signal from uninfected cells.

Figure S4

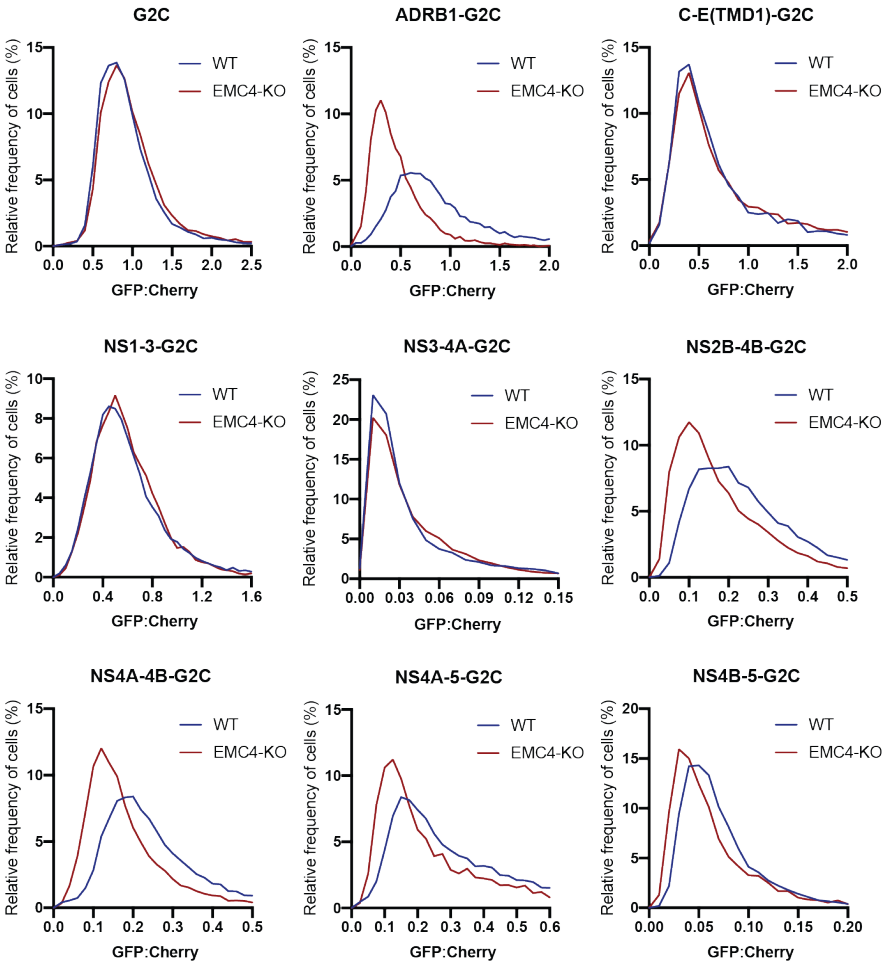

Figure S4: EMC is required for proper biogenesis of the NS4A-NS4B region of the DENV polyprotein

Flow cytometry measurements of GFP:mCherry fluorescence ratio for G2C constructs in WT and EMC4-KO HEK293FT cells. The fluorescence ratios are depicted as histograms. ADRB1=β_1-adrenergic receptor.

Figure S5

Virus isolate	Position	nt change	Coverage	Variant frequency	Reference frequency	aa change
EMC adapted DENV #3	226	T -> C	9754	99.80%	0.10%	synonymous
EMC adapted DENV #1	725	T -> C	5653	99.70%	0.10%	Val->Ala
EMC adapted DENV #1	1531	C -> T	3686	98.40%	0.80%	synonymous
EMC adapted DENV #2	1531	C -> T	9399	99.90%	0.10%	synonymous
EMC adapted DENV #3	1531	C -> T	14698	99.50%	0.20%	synonymous
EMC adapted DENV #1	1818	C -> A	3366	99.00%	0.20%	synonymous
EMC adapted DENV #3	4018	C -> T	16149	94.50%	5.50%	synonymous
EMC adapted DENV #2	5493	A -> G	10626	99.00%	0.50%	synonymous
EMC adapted DENV #1	6665	A -> G	3172	99.70%	0.10%	Tyr->Cys
EMC adapted DENV #2	6665	A -> G	8932	99.40%	0.50%	Tyr->Cys
EMC adapted DENV #3	6665	A -> G	13319	99.50%	0.20%	Tyr->Cys
EMC adapted DENV #1	7558	A -> T	4205	98.40%	0.40%	Asn->Tyr
EMC adapted DENV #2	7558	A -> T	10497	99.40%	0.10%	Asn->Tyr
EMC adapted DENV #3	7558	A -> T	16401	99.00%	0.04%	Asn->Tyr
EMC adapted DENV #3	7581	C -> T	16867	94.20%	5.70%	synonymous
EMC adapted DENV #3	8546	G -> A	15538	94.80%	5.10%	Arg->Lys

Figure S5: Adaptation of DENV to EMC-KO cells reveals conserved point mutations in NS4A and NS4B

Table containing all identified SNPs from the three isolated EMC-adapted viruses. A minimum variant frequency cutoff of 80% was used.

Material and methods

Cell culture and viruses

Huh7.5.1 (gift from Frank Chisari) and HEK293FT (Thermo Scientific) were cultured in DMEM (Gibco) supplemented with 10% fetal bovine serum (Omega Scientific), penicillin/streptomycin (Gibco), non-essential amino acids (Gibco) and L-glutamine (Gibco) at 37C and 5% CO_2. Parental cell lines were tested negative for mycoplasma. The following virus strains were used: DENV serotype 2 strain 16681 (stocks kindly provided by Caleb Marceau), DENV-Luc (stocks kindly provided by Jan Carette) (Marceau et al., 2016), WNV Kunjin strain CH16532 (stocks kindly provided by Jan Carette), ZIKV PRVABC59 (stocks kindly provided by Jan Carette) and HCV JFH1 (stocks kindly provided by Jan Carette). Viral titers were determined by plaque- or focus-forming assay.

Chemical compounds

MK-0608 (2'-C-Methylcytidine) was purchased from Carbosynth and used at a concentration of 25 µM. Bortezomib was obtained from Selleckchem and used at concentrations 1-50 nM. For all experiments, DMSO controls were included. Cycloheximide was purchased from Sigma and used at 100 µg/ml for Ribosome Profiling experiments.

Generation of knockout cell lines

Oligos containing sgRNA sequence were annealed and ligated into pX458 (gift from Feng Zhang; Addgene plasmid # 48138). Cells were transfected with pX458 using Lipofectamine 3000 (Invitrogen) and two days later GFP positive cells were single-cell sorted into 96-well plates using a Sony SH800 cell sorter. For genotyping, genomic DNA was isolated from obtained clones using QuickExtract (Lucigen), the sgRNA-targeted sites PCR amplified and the products Sanger-sequenced. Obtained sequences were compared to reference sequences for indel mutations. In the case of heterozygous mutations, TIDE was used to deconvolute sequencing traces (Brinkman

et al., 2014). A list of all used sgRNA oligo and genotyping primer sequences can be found in Supplementary Table 2.

Dengue Luciferase assay

Huh7.5.1 or HEK293FT cells were seeded in 96-well plates and infected with DENV-Luc at an moi of 0.01. Cells were harvested in Renilla Lysis buffer and luminescence was measured using Renilla Luciferase Assay system (Promega) on a Spectramax i3x Multi-Mode Microplate Reader (Molecular Devices).

Quantitative RT-PCR

Huh7.5.1 or HEK293FT cells were plated in 96-well plates (in triplicates for each condition) and infected with an moi of 0.5 for all viruses. Cells were then harvested at 30hpi for ZIKV, 48hpi for DENV and WNV, and 72hpi for HCV using the Power SYBR Cells-to-CT kit (Invitrogen). After reverse transcription, quantitative PCR was performed on a Bio-Rad CFX96 Touch system. All viral RNA levels were normalized to 18S levels. For viral internalization assay, 96-well plates containing WT or EMC4 KO Huh7.5.1 cells were put on ice before infection with DENV at an moi of 30. Cells were incubated for 1h before moving them to a 37C incubator. At each harvest timepoint, cells were washed three times with PBS and lysed as described above. All qPCR primer sequences can be found in Supplementary Table 2.

Lentiviral complementation

EMC2 (GenScript; clone OHu30604) and EMC4 cDNA (GenScript; clone OHu00964) were PCR amplified using tgtggtggaattctgcagataccATGGCGAAGGTCTCAGA / CGGCCGCCACTGTGCTGGATTTACTTATCGTCGTCATCCTTGTAATCAGACTGGGTGATC and tgtggtggaattctgcagataccATGACGGCCCAGGGG / CGGCCGCCACTGTGCTGGATTTACTTATCGTCGTCATCCTTGTAATCCAAAAGCAGTCCT,

525 respectively, and cloned into EcoRV-cut pLenti CMV Puro DEST (w118-1) (gift from Eric
526 Campeau & Paul Kaufman; Addgene plasmid # 17452) using NEBuilder® HiFi DNA Assembly
527 Master Mix (New England BioLabs). Lentivirus was produced in HEK293FT, respective KO cells
528 transduced with filtered, lentiviral containing supernatant and selected using 2-4 µg/ml puromycin
529 (Gibco) for 3-4 days.
530
531 ***Replicon assay***
532 DENV replicon plasmid (Marceau et al., 2016) was linearized using XbaI restriction enzyme.
533 Replicon RNA was generated using the MEGAscript T7 Kit (Invitrogen) with the reaction
534 containing 5mM m7G(5')ppp(5')G RNA Cap Structure Analog (New England BioLabs). Resulting
535 RNA was purified by lithium chloride precipitation. For electroporation, 2 million WT or EMC4 KO
536 HEK293FT cells were washed twice in PBS, resuspended in 100 µl SF Nucleofector solution
537 (Lonza), mixed with 4 µg replicon RNA, transferred to a 100ul nucleocuvette and pulsed using
538 program CM-130 on an Amaxa 4D-Nucleofector™ X Unit (Lonza). Cells were then resuspended
539 in antibiotic-free medium, distributed into 96-wells and lysed at different timepoints post-
540 electroporation using Renilla Lysis buffer. Luminescence was measured using Renilla Luciferase
541 Assay system (Promega) on a Spectramax i3x Multi-Mode Microplate Reader (Molecular
542 Devices).
543
544 ***Immunoblotting***
545 Cell were lysed using Laemmli SDS sample buffer containing 5% beta-mercaptoethanol and
546 boiled for 10min. Lysates were separated by SDS-PAGE on pre-cast Bio-Rad 4-15% poly-
547 acrylamide gels in Bio-Rad Mini-Protean electrophoresis system. Proteins were transferred onto
548 PVDF membranes using Bio-Rad Trans-Blot Turbo transfer system. PVDF membranes were
549 blocked with PBS buffer containing 0.1% Tween-20 and 5% non-fat milk. Blocked membranes
550 were incubated with primary antibody diluted in blocking buffer and incubated overnight at 4C on

a shaker. Primary antibodies were detected by incubating membranes with 1:10000 dilution of HRP-conjugated (Southern Biotech) or IRDye-conjugated (LI-COR) secondary anti-mouse and anti-rabbit antibodies for 1 h at room temperature. Blots were visualized using a ChemiDoc™ MP Imaging System (Bio-Rad). The following primary antibodies (and their dilutions) were used in this study: p84 (Genetex, GTX70220) at 1:2000, GAPDH (SCBT, sc-32233) at 1:2000, EMC2/TTC35 (Proteintech, 25443-1-AP) at 1:750, EMC4 (Bethyl, A305-752A) at 1:500, Dengue virus prM protein (Genetex, GTX128093) at 1:1000, Dengue virus Capsid protein (Genetex, GTX103343) at 1:1000, Dengue virus NS2B (Genetex, GTX124246) at 1:1000, Dengue virus NS3 protein (Genetex, GTX629477) at 1:1000, Dengue virus NS4B protein (Genetex, GTX124250) at 1:1000, Dengue virus Type 2 NS5 protein (Genetex, GTX629447) and GFP (Genetex, GTX113617) at 1:5000.

Ribosome profiling

WT and EMC4 KO HEK293FT were plated in 10cm dishes and infected with DENV at an of 100 for the 18hpi harvest and an moi of 0.5 for the 44hpi harvest. Cells were treated with 100 µg/ml cycloheximide for 2 min, washed once with polysome gradient buffer (20 mM Tris pH 7.5, 150 mM NaCl, 5 mM $MgCl_2$, 100 µg/mL cycloheximide, 1 mM DTT) and then lysed using 500 µl of polysome lysis buffer (20 mM Tris pH 7.5, 150 mM NaCl, 5 $MgCl_2$, 1% Triton X-100, 1 mM DTT, 100 µg/mL cycloheximide, 24 U/ml Turbo DNase (Ambion)) per plate. Cells/lysates were collected using cell scrapers and incubated on ice for 15min. Crude lysates were centrifuged at 20,000 x g for 2 min at 4C and the cleared polysome-containing lysates flash frozen by immersion in liquid nitrogen and stored at -80C until further processing. For ribosomal footprinting, 30 µg total RNA diluted in polysome buffer to a total volume of 200ul were treated with 750 U/ml RNaseI (Ambion) for 45min at 25C with shaking (300rpm). RNase activity was quenched by adding 10ul SuperaseIN (Invitrogen) and placing samples on ice. Note that 10% of the lysates were saved for RNA-seq library preparation (see below). A 1ml sucrose cushion was added to the bottom of a

13mm x 56mm thick-wall polycarbonate tube (Beckman Coulter) for each sample and the footprint digests were layered on top. Tubes were ultracentrifuged at 100,000 rpm for 4h at 4C in a TLA100.3 rotor (Beckman Coulter). After spin, supernatant was removed and the monosome-containing pellet was resuspended in 300 µl Trizol LS (Life Technologies) for RNA extraction using the Direct-Zol kit (Zymo). Ribosome Profiling NGS libraries were generated as previously described (Shurtleff et al., 2018).

For corresponding RNA-seq libraries RNA was extracted from the remaining undigested cleared lysates using Trizol and the Direct-Zol kit. 1 µg purified total RNA was used as input for the Truseq stranded total RNA Gold library prep (Illumina). Ribosomal RNA was depleted using Ribo-Zero H/M/R Gold and depleted RNA fragmented for 8min at 94C. Following first and second strand synthesis products were purified using SPRI beads. KAPA dual-indexed adapters (Kapa Biosystems, KK8722) were used for adapter ligation. Finally, PCR enriched products were cleaned up using SPRI. Ribosome Profiling and RNA-seq libraries were analyzed on Bioanalyzer or TapeStation (Agilent) before sequencing on a NextSeq 500 platform (Illumina) in separate runs with 400M reads output.

Analysis of Ribosome Profiling data

Reads from Ribosome Profiling or RNA-seq were preprocessed by removing low-quality reads and trimming of adaptor sequences. Next, ribosomal RNA reads were removed using Bowtie. Remaining reads were aligned to the human reference genome file also containing the genomic DENV2 16681 sequence using Tophat to generate read count tables with RPKMs for each transcript. A cutoff of at least 5 RPKMs was used for further analysis of transcripts/footprint counts, and $\log_2$ fold-changes (FC) were calculated between corresponding EMC4 KO and WT samples for both Ribosome Profiling and RNA-seq. To calculate translation efficiency (TE), the Ribosome Profiling RPKMs were normalized by the RNA-seq RPKMs for each transcript.

602 To analyze the footprint distribution of Ribosome Profiling reads across the DENV genome, DENV
603 specific reads were mapped to the DENV2 16681 reference sequence using Geneious Prime and
604 coverage at each nucleotide position was determined.
605
606 ***Dual fluorescence cytometry assay***
607 eGFP was amplified from pX458 with adding overhang to plenti-CMV-Puro (EcoRV cut site), a
608 Kozak sequence and ATG start codon for the G2C-only construct or with an additional overhang
609 to GlySer-linker sequence for fusion with DENV fragments. T2A-mCherry was amplified from
610 pX458 where eGFP had been replaced with mCherry. Different regions of the DENV genome
611 were amplified from the DENV2 16681 infectious clone plasmid (gift from Karla Kirkegaard) with
612 addition of overhang sequences to plenti-CMV backbone, Kozak sequence and ATG start codon
613 on 5'end and to GlySer-linker-GFP fragment on 3'end. ADRB1 was amplified from pcDNA3 Flag
614 beta-1-adrenergic-receptor (gift from Robert Lefkowitz; Addgene plasmid # 14698). All fragments
615 contained ~20bp overhangs and were assembled into EcoRV cut pLenti CMV Puro DEST (w118-
616 1) using NEBuilder® HiFi DNA Assembly Master Mix (New England BioLabs) or Gibson-like
617 master mix (Berkeley MacroLabs) to generate G2C reporter expression constructs. All constructs
618 were verified by Sanger sequencing. Primer sequences can be found in Supplementary Table 2.
619 For the G2C dual fluorescence assay, cells were seeded in 24- or 12-well plates and transfected
620 with G2C constructs using Lipofectamine 3000 (Invitrogen). 24-48h later cells were trypsinized,
621 filtered (70µm), and analyzed by flow cytometry using a Cytoflex S flow cytometer (Beckman
622 Coulter). At least 5,000 and 10,000 mCherry positive cells were recorded for Huh7.5.1 and
623 HEK293FT, respectively. For analysis, cells were gated based on FSC/SSC, FSC-H/FSC-A
624 (singlets) and finally ECD (mCherry) and FITC (eGFP) using FlowJo 10. Raw fluorescence data
625 for all gated fluorescent cells was exported and the eGFP:mCherry intensity ratios were calculated
626 for individual cells. All fluorescence ratios were normalized to the mean of the G2C-only construct.
627 Distributions of fluorescence ratios were plotted as histograms using GraphPad Prism 8.

628

629 ***Viral adaptation***

630 WT DENV serotype 2 strain 16681 was serially passaged every 3-4 days onto newly plated EMC4
631 KO Huh7.5.1 cells by transferring increasingly diluted supernatant from infected cells (starting at
632 2-fold dilutions for the first 3 passages, then stepwise increase of dilutions to 100-fold for the final
633 passages). Six independent passaging experiments were started and cytopathic effects were
634 observed in three of the replicates after approximately 20-22 passages. Supernatant was then
635 harvested, filtered through a 0.45 um filter to remove cellular debris, and RNA was extracted using
636 Trizol LS and Direct-Zol kit (Zymo). Additionally, RNA was extracted from WT DENV stock. To
637 prepare sequencing libraries, Truseq stranded total RNA Gold library kit (Illumina) was used.
638 Isolated RNA was fragmented for 4min at 94C without prior Ribo-Zero depletion, followed by first
639 and second strand synthesis, and adapter ligation. Fragments were amplified in presence of
640 SYBR Green on Bio-Rad CFX96 and reaction was stopped for each sample before it reached
641 plateau (~20-24 cycles). Libraries from different virus isolates were pooled and sequenced on
642 iSeq 100 (Illumina) with 2x75bp reads.
643 For analysis, Geneious Prime was used: Fastq files were imported as paired reads and Truseq
644 adapters and low-quality sequences (minimum 20) were trimmed using BBDuk. Next, reads were
645 mapped to the WT 16681 reference genome using the Geneious Mapper at medium-low
646 sensitivity and with 5 iterations for fine-tuning. All samples had a minimum coverage of 1000 at
647 all nucleotide positions. Finally, SNPs between adapted and WT stock viruses were called with a
648 minimum variance frequency of 80%. To compare acquired non-synonymous point mutations to
649 a large dataset of sequenced DENV2 strains, 1,359 complete genome sequences from NCBI
650 were mapped to the DENV2 16681 strain containing adapted mutations.

651

652 ***Generation of EMC adapted DENV-Luciferase***

653 DENV-Luc infectious clone containing adapted mutations were generated by PCR amplification
654 from WT DENV-Luc infectious clone plasmid (gift from Jan Carette). For DENV-Luc(A6665G)
655 fragments were amplified using GAAGAGTGATGGTTATGGTAGGC /
656 CTGTATTTGTGCGCACCATAGGAGGATG and CATCCTCCTATGGTGCGCACAAATACAG /
657 GTGATCTTCATTTAAGAATCCTAGGGCTTC. For DENV-Luc(A7558T) fragments were
658 amplified using GAAGAGTGATGGTTATGGTAGGC / CCCCTTCTTGTGTAGGTTGTGTTCTTC
659 and GAAGAACACAACCTACACAAGAAGGGG / GTGATCTTCATTTAAGAATCCTAGGGCTTC.
660 For DENV-Luc(A6665G, A7558T) fragments were amplified using
661 GAAGAGTGATGGTTATGGTAGGC / CTGTATTTGTGCGCACCATAGGAGGATG,
662 CATCCTCCTATGGTGCGCACAAATACAG / CCCCTTCTTGTGTAGGTTGTGTTCTTC, and
663 GAAGAACACAACCTACACAAGAAGGGG / GTGATCTTCATTTAAGAATCCTAGGGCTTC.
664 PCR products were cloned into NarI and AvrII cut WT DENV-Luc infectious clone using
665 NEBuilder® HiFi DNA Assembly Master Mix (New England BioLabs) and transformed into Stbl3
666 bacteria (Berkeley MacroLabs). Constructs were verified by Sanger sequencing. Plasmids were
667 linearized with XbaI and RNA was generated by in-vitro transcription using the MEGAscript T7 Kit
668 (Invitrogen) with the reaction containing 5mM m7G(5')ppp(5')G RNA Cap Structure Analog (New
669 England BioLabs). Resulting RNA was purified by lithium chloride precipitation and transfected
670 into BHK-21 cells using Lipofectamine 3000 for viral production. Supernatants were harvested 6-
671 9 days post-transfection.
672
673 ***Co-immunoprecipitation***
674 HEK293FT EMC4 KO cells complemented with FLAG-tagged EMC4 were seeded in a 10cm dish
675 and infected with DENV for 96h. Cells were washed with PBS and then collected in 1ml Pierce
676 RIPA buffer (Thermo Scientific) containing 1mM PMSF (Thermo Scientific), 5mM EDTA and 1x
677 Halt Protease Inhibitor Cocktail (Thermo Scientific) with help of cell scrapers. Cells were lysed on
678 ice for 1h with occasional vortexing and subsequently centrifuged at 15,000 x g for 10min at 4C

679 to clear lysates. For co-immunoprecipitation, clarified lysates were incubated at 4C overnight with
680 Anti-FLAG® M2 Magnetic Beads (Sigma) while rotating. Beads were washed three times using
681 TBS-T and eluted by boiling in 2x Laemmli buffer. Eluates were loaded for SDS-PAGE and stained
682 for viral proteins.
683
684 ***Statistical analysis***
685 GraphPad Prism 8 was used to analyze data and perform statistical tests. Unpaired *t*-tests were
686 applied to measure statistical significance of differences in DENV infection between WT and EMC
687 KO cells.
688
689 **Supplementary tables**
690 ***Supplementary Table 1***
691 Ribosome Profiling data including read counts and fold change for Ribosome Profiling and RNA-
692 seq used to generate Figures 3A-C.
693
694 ***Supplementary Table 2***
695 Table of oligos used in this study: sgRNA oligos, genotyping primers, qPCR primers, primers to
696 generate G2C constructs
697
698

References

Abernathy, E., Mateo, R., Majzoub, K., van Buuren, N., Bird, S.W., Carette, J.E., and Kirkegaard, K. (2019). Differential and convergent utilization of autophagy components by positive-strand RNA viruses. PLoS Biol. *17*, e2006926.

Beaucourt, S., and Vignuzzi, M. (2014). Ribavirin: a drug active against many viruses with multiple effects on virus replication and propagation. Molecular basis of ribavirin resistance. Curr. Opin. Virol. *8*, 10–15.

Brinkman, E.K., Chen, T., Amendola, M., and van Steensel, B. (2014). Easy quantitative assessment of genome editing by sequence trace decomposition. Nucleic Acids Res. *42*, e168–e168.

Chen, Y.-L., Yokokawa, F., and Shi, P.-Y. (2015). The search for nucleoside/nucleotide analog inhibitors of dengue virus. Antiviral Res. *122*, 12–19.

Chitwood, P.J., and Hegde, R.S. (2019). The Role of EMC during Membrane Protein Biogenesis. Trends Cell Biol.

Chitwood, P.J., Juszkiewicz, S., Guna, A., Shao, S., and Hegde, R.S. (2018). EMC Is Required to Initiate Accurate Membrane Protein Topogenesis. Cell *175*, 1507-1519.e16.

Christianson, J.C., Olzmann, J.A., Shaler, T.A., Sowa, M.E., Bennett, E.J., Richter, C.M., Tyler, R.E., Greenblatt, E.J., Harper, J.W., and Kopito, R.R. (2011). Defining human ERAD networks through an integrative mapping strategy. Nat. Cell Biol. *14*, 93–105.

Coelho, J.P.L., Stahl, M., Bloemeke, N., Meighen-Berger, K., Alvira, C.P., Zhang, Z.-R., Sieber, S.A., and Feige, M.J. (2019). A network of chaperones prevents and detects failures in membrane protein lipid bilayer integration. Nat. Commun. *10*.

Guna, A., Volkmar, N., Christianson, J.C., and Hegde, R.S. (2018). The ER membrane protein complex is a transmembrane domain insertase. Science *359*, 470–473.

Ingolia, N.T., Ghaemmaghami, S., Newman, J.R.S., and Weissman, J.S. (2009). Genome-Wide Analysis in Vivo of Translation with Nucleotide Resolution Using Ribosome Profiling. Science *324*, 218–223.

Jonikas, M.C., Collins, S.R., Denic, V., Oh, E., Quan, E.M., Schmid, V., Weibezahn, J., Schwappach, B., Walter, P., Weissman, J.S., et al. (2009). Comprehensive characterization of genes required for protein folding in the endoplasmic reticulum. Science *323*, 1693–1697.

Krishnan, M.N., Ng, A., Sukumaran, B., Gilfoy, F.D., Uchil, P.D., Sultana, H., Brass, A.L., Adametz, R., Tsui, M., Qian, F., et al. (2008). RNA interference screen for human genes associated with West Nile virus infection. Nature *455*, 242–245.

Lee, Y.-R., Kuo, S.-H., Lin, C.-Y., Fu, P.-J., Lin, Y.-S., Yeh, T.-M., and Liu, H.-S. (2018). Dengue virus-induced ER stress is required for autophagy activation, viral replication, and pathogenesis both in vitro and in vivo. Sci. Rep. *8*, 489.

735 Lin, C., Amberg, S.M., Chambers, T.J., and Rice, C.M. (1993). Cleavage at a novel site in the
736 NS4A region by the yellow fever virus NS2B-3 proteinase is a prerequisite for processing at the
737 downstream 4A/4B signalase site. J. Virol. *67*, 2327–2335.

738 Ma, H., Dang, Y., Wu, Y., Jia, G., Anaya, E., Zhang, J., Abraham, S., Choi, J.-G., Shi, G., Qi, L.,
739 et al. (2015). A CRISPR-Based Screen Identifies Genes Essential for West-Nile-Virus-Induced
740 Cell Death. Cell Rep. *12*, 673–683.

741 Marceau, C.D., Puschnik, A.S., Majzoub, K., Ooi, Y.S., Brewer, S.M., Fuchs, G., Swaminathan,
742 K., Mata, M.A., Elias, J.E., Sarnow, P., et al. (2016). Genetic dissection of Flaviviridae host
743 factors through genome-scale CRISPR screens. Nature *535*, 159–163.

744 Miller, S., Sparacio, S., and Bartenschlager, R. (2006). Subcellular Localization and Membrane
745 Topology of the Dengue Virus Type 2 Non-structural Protein 4B. J. Biol. Chem. *281*, 8854–
746 8863.

747 Miller, S., Kastner, S., Krijnse-Locker, J., Bühler, S., and Bartenschlager, R. (2007). The Non-
748 structural Protein 4A of Dengue Virus Is an Integral Membrane Protein Inducing Membrane
749 Alterations in a 2K-regulated Manner. J. Biol. Chem. *282*, 8873–8882.

750 Muñoz-Jordán, J.L., Laurent-Rolle, M., Ashour, J., Martínez-Sobrido, L., Ashok, M., Lipkin, W.I.,
751 and García-Sastre, A. (2005). Inhibition of alpha/beta interferon signaling by the NS4B protein of
752 flaviviruses. J. Virol. *79*, 8004–8013.

753 Neufeldt, C.J., Cortese, M., Acosta, E.G., and Bartenschlager, R. (2018). Rewiring cellular
754 networks by members of the Flaviviridae family. Nat. Rev. Microbiol. *16*, 125–142.

755 Olzmann, J.A., Kopito, R.R., and Christianson, J.C. (2013). The Mammalian Endoplasmic
756 Reticulum-Associated Degradation System. Cold Spring Harb. Perspect. Biol. *5*.

757 Peña, J., and Harris, E. (2011). Dengue virus modulates the unfolded protein response in a
758 time-dependent manner. J. Biol. Chem. *286*, 14226–14236.

759 Puschnik, A.S., Marceau, C.D., Ooi, Y.S., Majzoub, K., Rinis, N., Contessa, J.N., and Carette,
760 J.E. (2017). A Small-Molecule Oligosaccharyltransferase Inhibitor with Pan-flaviviral Activity.
761 Cell Rep. *21*, 3032–3039.

762 Reid, D.W., Campos, R.K., Child, J.R., Zheng, T., Chan, K.W.K., Bradrick, S.S., Vasudevan,
763 S.G., Garcia-Blanco, M.A., and Nicchitta, C.V. (2018). Dengue Virus Selectively Annexes
764 Endoplasmic Reticulum-Associated Translation Machinery as a Strategy for Co-opting Host Cell
765 Protein Synthesis. J. Virol. *92*, e01766-17.

766 Roosendaal, J., Westaway, E.G., Khromykh, A., and Mackenzie, J.M. (2006). Regulated
767 cleavages at the West Nile virus NS4A-2K-NS4B junctions play a major role in rearranging
768 cytoplasmic membranes and Golgi trafficking of the NS4A protein. J. Virol. *80*, 4623–4632.

769 Savidis, G., McDougall, W.M., Meraner, P., Perreira, J.M., Portmann, J.M., Trincucci, G., John,
770 S.P., Aker, A.M., Renzette, N., Robbins, D.R., et al. (2016). Identification of Zika Virus and
771 Dengue Virus Dependency Factors using Functional Genomics. Cell Rep. *16*, 232–246.

772 Senft, D., and Ronai, Z.A. (2015). UPR, autophagy, and mitochondria crosstalk underlies the
773 ER stress response. Trends Biochem. Sci. *40*, 141–148.

774 Sessions, O.M., Barrows, N.J., Souza-Neto, J.A., Robinson, T.J., Hershey, C.L., Rodgers, M.A.,
775 Ramirez, J.L., Dimopoulos, G., Yang, P.L., Pearson, J.L., et al. (2009). Discovery of insect and
776 human dengue virus host factors. Nature *458*, 1047–1050.

777 Shao, S., and Hegde, R.S. (2011). Membrane Protein Insertion at the Endoplasmic Reticulum.
778 Annu. Rev. Cell Dev. Biol. *27*, 25–56.

779 Shurtleff, M.J., Itzhak, D.N., Hussmann, J.A., Oakdale, N.T.S., Costa, E.A., Jonikas, M.,
780 Weibezahn, J., Popova, K.D., Jan, C.H., Sinitcyn, P., et al. (2018). The ER membrane protein
781 complex interacts cotranslationally to enable biogenesis of multipass membrane proteins. ELife
782 *7*, e37018.

783 Su, H.-L., Liao, C.-L., and Lin, Y.-L. (2002). Japanese Encephalitis Virus Infection Initiates
784 Endoplasmic Reticulum Stress and an Unfolded Protein Response. J. Virol. *76*, 4162–4171.

785 Volkmar, N., Thezenas, M.-L., Louie, S.M., Juszkiewicz, S., Nomura, D.K., Hegde, R.S.,
786 Kessler, B.M., and Christianson, J.C. (2019). The ER membrane protein complex promotes
787 biogenesis of sterol-related enzymes maintaining cholesterol homeostasis. J. Cell Sci. *132*.

788 Zhang, R., Miner, J.J., Gorman, M.J., Rausch, K., Ramage, H., White, J.P., Zuiani, A., Zhang,
789 P., Fernandez, E., Zhang, Q., et al. (2016). A CRISPR screen defines a signal peptide
790 processing pathway required by flaviviruses. Nature *535*, 164–168.

791 Zou, J., Lee, L.T., Wang, Q.Y., Xie, X., Lu, S., Yau, Y.H., Yuan, Z., Geifman Shochat, S., Kang,
792 C., Lescar, J., et al. (2015). Mapping the Interactions between the NS4B and NS3 proteins of
793 dengue virus. J. Virol. *89*, 3471–3483.

794